VALIDATION OF A MOLTEN SALT PARABOLIC TROUGH RECEIVER MODEL BASED ON AN EMPIRICAL HEAT LOSS MODEL

Christoph A. Pan[1], Frank Dinter[1], and Thomas M. Harms[1]

[1] Solar Thermal Energy Research Group (STERG), Stellenbosch University, Private Bag X1, 7602, Matieland, South Africa; Phone: +27 (0)21 808 4016; Fax: +27 (0)21 808 4933; Email: cpan@sun.ac.za, frankdinter@sun.ac.za, tmh@sun.ac.za

Abstract

This study describes the development, validation and improvement of a molten salt parabolic trough receiver model based on an empirically determined heat loss model for the use in a multi-objective optimization study. The results show that, for three investigated heat transfer fluids, i.e. Solar Salt, Hitec, and Hitec XL, there is a good agreement between the new model and the model used for the validation. A parameter study showed that a time step size of 60 minutes and a discretization of one control volume per solar collector array within a loop is sufficiently accurate and reduces the required simulation time significantly. Further adaptations have been implemented into the model to facilitate the characteristics of molten salts as heat transfer fluids with their resulting requirements for the operating strategy of the solar field, including a recirculation from the cold storage tank and an increased night time flow rate compared to the minimum diurnal flow rate during standby operation.

Keywords: parabolic trough; molten salt; empirical heat loss model; transient modelling; model validation.

1. Introduction

Power plants using parabolic trough (PT) technology with thermal oils as heat transfer fluids (HTF) are state of the art. In order to achieve higher power cycle efficiencies, higher temperature differences are necessary. Because the upper operating temperature is limited for thermal oils by their thermal stability limit, other HTFs like e.g. molten salts (MS) can be used. The open-source simulation software System Advisor Model (SAM) [1] from the National Renewable Energy Laboratory (NREL) is widely considered as a well validated [2] tool in academia for performance analyses of CSP plants. Although the software allows the use of commercially available molten salts like Hitec Solar Salt, Hitec and Hitec XL, the operating strategy and control system is not advantageous for this type of HTF. The original intention of use was for thermal oils, which have a considerably lower freezing temperature than molten salts (12 °C compared to between 120 and 220 °C depending on the salt mixture), making the need to continuously

recirculate the HTF through the solar field at night a less prioritized requirement. However, molten salts are limited by their high freezing temperature. One possible freeze protection method is to recirculate the fluid from the cold storage tank. SAM does not offer the option to direct the HTF from the solar field outlet to the cold storage tank but rather circulates it directly back to the solar field. Thus, an improved operating control allowing the recirculation from the cold storage tank is required.

The model developed in this study is based on the system of equations of SAM with the difference that it uses an empirically determined heat loss model as suggested by researchers in reference [3]. Instead of being solely based on a physical energy balance as in Fig. 1 (a), the energy balance for the newly developed model is simplified according to Fig. 1 (b) by using a correlation developed by Matino & Maccari [4] to calculate the receiver heat losses based on its absorber tube surface temperature. This simplification reduces the set of equations and iterations to determine the heat losses, which in return shortens the simulation time. This is beneficial when conducting multi-objective optimization studies, which typically consist of several thousand annual simulations to determine a set of optimal solutions (pareto-optimal front) for various optimization objectives and input variables. Reducing the computational effort necessary each annual simulation can reduce the overall simulation time significantly.

Another limiting factor of SAM is the discretization of the solar collector arrays (SCAs) into only one node per SCA. As shown by researchers in references [3] and [5], a smaller spatial resolution of the SCAs leads to a more confident representation of the transient response of the solar field. When using molten salts, a precise prediction of the solar field's thermal inertia is necessary to accurately predict when the freeze protection (FP) system needs to be activated to avoid freezing.

2. Methodology and model development

The model presented in this paper was developed within TRNSYS with the code for the parabolic trough written in

Fortran and pre- and post-processing in MATLAB. The energy balances and temperature calculations in section 2.1 are mainly based on the equations used in SAM as reported in reference [6] with some exceptions, which are described in more detail in the following sections. The heat transfer fluids investigated in this study are Hitec Solar Salt (herein referred to as 'Solar Salt' for convenience), Hitec and Hitec XL with their thermo-physical properties. The solar field (SF) is formed by the FLABEG Ultimate Trough® collector in combination with Archimede Solar Energy's HCEMS-11 receiver tubes, specifically developed for the use with molten salts for high temperature applications of up to 550 °C [7].

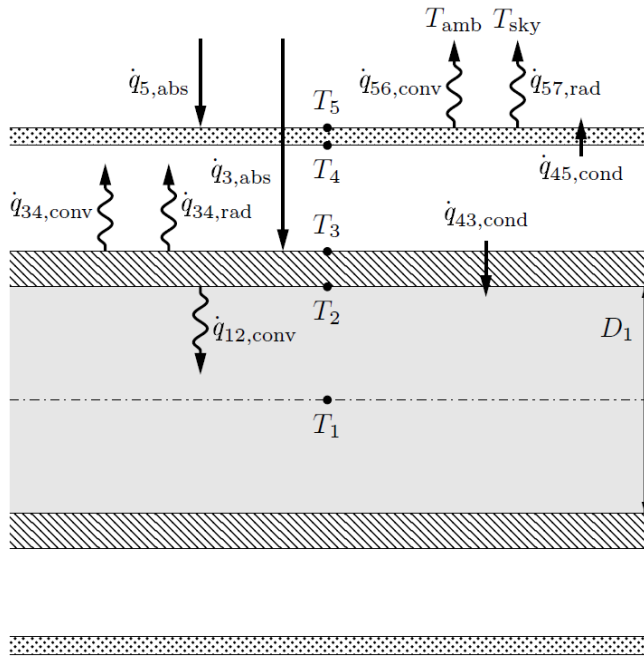## 2.1. Energy balance of the receiver

Parabolic trough power plants require a transient simulation based on an energy balance that considers the thermal inertia of the mass of the HTF and steel in the solar field to accurately model the thermal behaviour. The transient effect on the change of internal energy of the HTF and steel mass greatly impacts the SF performance and is included in the energy balance as

$$\dot{q}_{\text{in}} + \dot{q}_{\text{conv}} = \frac{\partial U}{\partial t} + \dot{q}_{\text{out}} \qquad \text{(Eq. 1)}$$

with the general transient change in internal energy of the HTF as a function of time t

$$\frac{\partial U}{\partial t} = (m_{\text{HTF}}\, c_{p,\text{HTF}} + m_{\text{tube}}\, c_{p,\text{tube}}) \frac{\partial T}{\partial t} \qquad \text{(Eq. 2)}$$

where the terms m and c_p are the mass and specific heat capacity

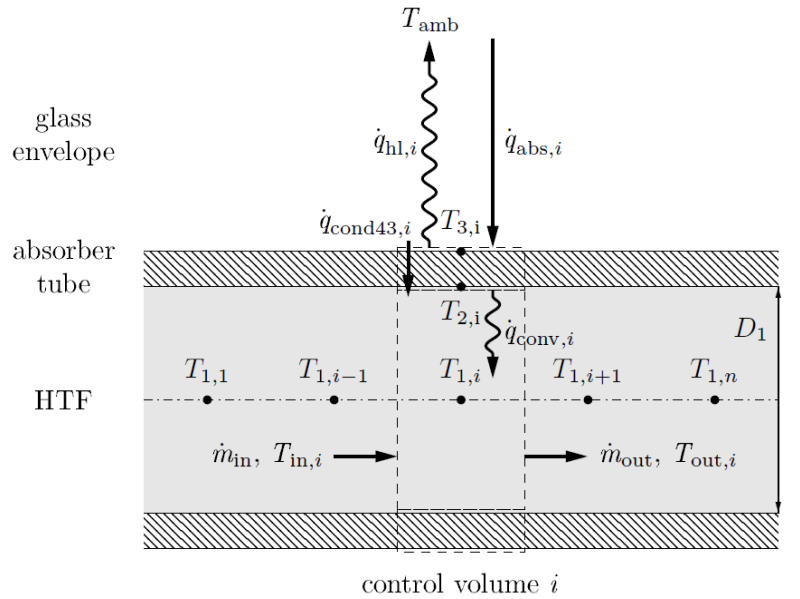of the HTF and the absorber tube, respectively. The longitudinal inlet and outlet energy flows can be expressed as

$$\dot{q}_{\text{in}} - \dot{q}_{\text{out}} = \dot{m}_{HTF}\, c_{p,\text{HTF}}\, (T_{\text{in}} - T_{\text{out}}) \qquad \text{(Eq. 3)}$$

with T_{in} and T_{out} being the inlet and outlet temperature, respectively. To approximate the unknown outlet temperature, each loop was discretized into n finite control volumes (CV) along the flow direction; in this case, one control volume i per SCA with a nodal fluid temperature $T_{1,i}$ and an inner and outer absorber tube surface temperature $T_{2,i}$ and $T_{3,i}$ as in Fig. 1 (b). The thermal capacity is assumed to be lumped within each CV and the HTF properties are evaluated at each time step as a function of temperature of the respective node i. The same principle was also applied to the header and runner piping of the solar field but were treated as a single node. The absorbed thermal power of the HTF $\dot{q}_{\text{conv}}$ in Eq. 1 is expressed for each control volume i along the loop as

$$\text{for } i = 1, n \begin{cases} \dot{q}_{conv,i} = \dot{q}_{\text{abs},i} - \dot{q}_{\text{hl},i} & \text{(Eq. 4)} \\ \dot{q}_{\text{abs},i} = I_b\, A_i\, \eta_{\text{col},i}\, \eta_{\text{rec},i} & \text{(Eq. 5)} \end{cases}$$

where $\dot{q}_{\text{abs},i}$ is the absorbed thermal power of the absorber tube with the beam irradiance I_b, the aperture area A_i, the collector efficiency $\eta_{\text{col},i}$ and the receiver efficiency $\eta_{\text{rec},i}$. Due to the dominance of the radiative heat transfer, a simplified heat loss model as in Fig. 1 (b) is sufficient, where heat loss $\dot{q}_{\text{hl},i}$ for the HCEMS-11 receiver as a function of the receiver outer surface temperature $T_{3,i}$ has been correlated by Matino & Maccari [4] as

$$\dot{q}_{\text{hl},i} = c_1\, T_{3,i} + c_4\, T_{3,i}^4 \qquad \text{(Eq. 6)}$$

(a)   (b)

Fig. 1. Steady-state energy balance for (a) a physical receiver model and (b) the simplified empirical heat loss model

with the receiver performance coefficients c_1 and c_4 as per Table 1. However, as the outlet fluid temperature $T_{\text{out},i}$ of each control volume depends on the receiver heat losses as a function of the absorber temperature $T_{3,i}$ and vice versa, the model uses the "regula falsi" method to approximate the two temperatures within a tolerance of 0.001 based on appropriate initial guess values.

The mass flow rate is calculated through an iterative feedback controller in TRNSYS, which uses a secant method in combination with successive substitution to find the appropriate flow rate within the defined limits in order to keep the solar field outlet temperature close to the set point.

Receiver condition	c_1	c_4
Vacuum in annulus	0.19	7.8×10^{-9}
Air in annulus (~0.1 mbar)	0.5	7.9×10^{-9}
Vacuum lost	1.01	8×10^{-9}

Table 1. Receiver performance coefficients [4]

2.2. Convective heat transfer model

Each control volume i is coupled to a one-dimensional convective heat transfer model, which is only applicable to the HTF in this case. The wall-to-fluid convection heat transfer coefficient h of the HTFs is calculated from Eq. 7 during each time step with

$$h_i = \frac{Nu_i\, k_{\text{HTF},i}}{d} \qquad \text{(Eq. 7)}$$

where Nu_i is the Nusselt number, $k_{\text{HTF},i}$ the thermal conductivity of the fluid and d the characteristic length, which is the inner tube diameter D_1 in this case. Wu *et al.* [8] developed correlations as functions of the Reynolds number Re_i and the Nusselt number Nu_i for molten salts from experimental data for transition flow Eq. 8 and turbulent flow Eq. 9. Both equations

are valid for $1.6 < Pr_i < 23.9$.

$$Nu_i = \begin{cases} 0.00154\, Re_i^{1.1}\, Pr_i^{1/3}, & 2300 < Re_i < 10^4 \quad \text{(Eq. 8)} \\ 0.02948\, Re_i^{0.787}\, Pr_i^{1/3}, & Re_i \geq 10^4 \quad \text{(Eq. 9)} \end{cases}$$

The Reynolds number Re_i is calculated from Eq. 10 with the bulk fluid density ρ_i, the average fluid velocity v_i, the pipe inner diameter D_1 and the dynamic viscosity μ_i. The Prandtl number Pr_i is obtained from Eq. 11 with the bulk specific heat capacity $c_{\text{HTF},i}$ of the fluid.

$$Re_i = \frac{\rho_i\, v_i\, D_1}{\mu_i} \quad \text{(Eq. 10)} \qquad Pr_i = \frac{c_{p,\text{HTF},i}\, \mu_i}{k_{\text{HTF},i}} \quad \text{(Eq. 11)}$$

Fig. 2 shows the Reynolds numbers of the investigated HTFs as a function of the fluid temperature and their respective thermo-physical properties at an inner tube diameter of $D_1 = 0.064$ m and a velocity of $v = 1$ m/s. This corresponds to the diameter of the investigated receiver tubes and a velocity that represents a typical flow rate of the HTF during operation. For the chosen conditions, only Hitec XL is not above the limit of $Re_i > 10^4$. However while the solar field is in operation, the fluid temperature is above 290 °C (533.15 K) and thus does not invalidate the condition for turbulent flow. The Reynolds number only falls below 10^4 during times when the solar field is on standby and does not therefore reduce the heat transfer coefficient during operation.

For the same conditions, Fig. 3 shows the heat transfer coefficient of the three HTFs. Solar Salt and Hitec both generally have a higher heat transfer coefficient than Hitec XL, whereby Solar Salt's higher operating temperature enables higher heat transfer coefficients. At low temperatures, the heat transfer coefficient of Hitec XL also reduces due to the transitional flow. However, this is in fact favourable as it reduces the heat loss when the fluid velocity is low when the solar field is not operational like e.g. at night or during standby.
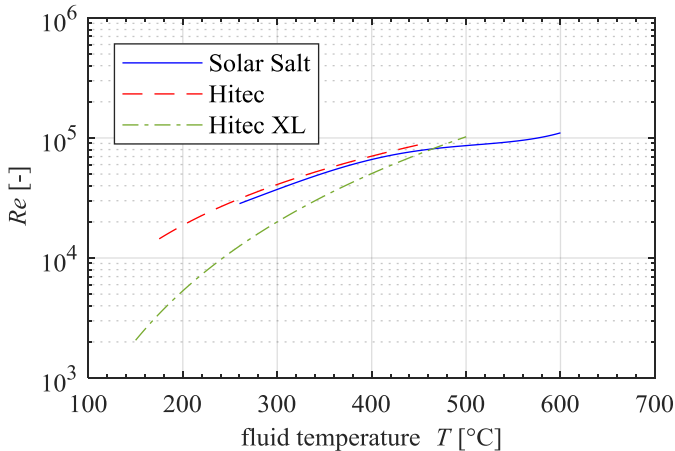

Fig. 2. Reynolds numbers of HTFs as a function of fluid temperature at $D_1 = 0.064$ m and $v_i = 1$ m/s
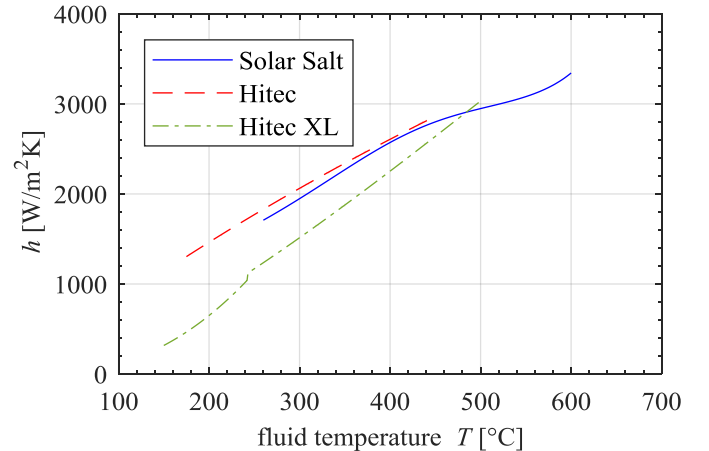

Fig. 3. Heat transfer coefficients of HTFs as a function of fluid temperature at $D_1 = 0.064$ m and $v_i = 1$ m/s

2.3. Solar field control

As SAM only allows to specify a minimum and maximum flow rate for the pumps, the solar field control was also modelled accordingly. Nevertheless, this was implemented as two operating modes (OM) plus a third one for a dedicated night time mode for later use in section 4:

- OM1: standby circulation (2 kg/s)
- OM2: design circulation (min. – max. kg/s)
- OM3: night circulation (4 kg/s)

2.4. Assumptions and simplifications

To summarize, the model is based on the following assumptions and simplifications:

- The fluid is assumed to be homogenously mixed within each discrete control volume i where the thermal capacitance is assumed to be lumped at the central node.
- All fluid properties are functions of the bulk temperature of the node in the centre of the tube.
- The material properties of the absorber tube are assumed to be constant across the loop.
- The solar flux on the receiver is assumed to be uniform circumferentially and longitudinally. Therefore, the circumferential temperatures are also assumed to be uniform.
- The longitudinal and circumferential heat transfer of the receiver and fluid are neglected.
- Heat losses from the expansion bellows and support brackets are neglected.

3. Model validation

The model was validated with SAM as it is freely available and widely used for performance analyses of CSP plants. The validation approach and results are presented hereafter.

3.1. Simulation setup

To warrant comparability of the two models, the following measures were taken to set up the simulations. Firstly, the identical weather data set in form of a typical meteorological year (TMY3) for Upington, South Africa, was used in both models; including, inter alia, the direct normal irradiance (DNI),

ambient temperature and atmospheric pressure. Secondly, the same geometric, physical and thermal properties were implemented in both models for the main solar field components, i.e. the collectors and receivers. Thirdly, the input parameters for the plant control and any other relevant system variable were set to the same values in both models to ensure comparability. Likewise, parameters relevant for the simulation solver, i.e. simulation time step size and control volume size (nodes per SCA), were set to equal values. Fourthly, to eliminate the impact of a different HTF recirculation strategy within the two models, the inlet temperature for the solar field from SAM was used as an input variable to the new model. Furthermore, SAM does not allow to specify a night time flow rate higher than the minimum flow rate. The effects of the two different recirculation strategies on the solar field operation and a newly introduced night time flow rate are analysed in more detail in section 4. The design point parameters of both models for the performance calculations at design are listed in Table 2.

Parameter	Unit	Value		
Time step size	Min	60		
CV per SCA	-	1		
DNI at design	W/m²	850		
Solar multiple	-	1.6		
SF inlet temperature	°C	290		
Min flow rate per loop	kg/s	2		
Heat transfer fluid	-	Solar Salt	Hitec	Hitec XL
SF outlet temperature	°C	550	450	450
FP temperature	°C	260	170	150
Max flow rate per loop	kg/s	10.2	18.1	19.8

Table 2. Design point parameters

3.2. Results and discussion

Table 3 lists the design point performances for the various HTFs in SAM and the new model. The receiver heat losses and SF thermal power both have low error of maximal 0.64 %. However, large errors of up to 13.48 % occur for the SF heat loss because of the different calculation methods within the two models. Hitec and Hitec XL have the same design point heat loss because they have the same design solar field outlet temperature of 450 °C, whereas Solar Salt has higher heat losses due to its higher operating temperature of 550 °C. The SF conversion efficiency also shows acceptable errors for all HTFs.

For the validation, annual simulations with the various HTFs

Heat transfer fluid		Solar Salt			Hitec			Hitec XL		
Performance at design	Unit	SAM	Model	Relative error	SAM	Model	Relative error	SAM	Model	Relative error
Receiver heat loss	W/m	312.3	311.9	**0.13 %**	209.8	210.0	**0.10 %**	209.8	210.0	**0.10 %**
SF thermal power	MW$_{th}$	225.6	224.8	**0.37 %**	231.6	230.1	**0.64 %**	231.6	230.5	**0.47 %**
SF heat loss	MW$_{th}$	16.4	17.1	**4.11 %**	10.5	11.9	**13.48 %**	10.5	11.4	**8.71 %**
SF conversion efficiency	%	70.20	68.82	**1.97 %**	71.48	70.42	**1.48 %**	71.48	70.56	**1.29 %**

Table 3. Comparison of the design point performances in SAM and the new model

were carried out in both models. The results were then compared in terms of the mean absolute error (MAE), which are presented in Table 4 and discussed in more detail hereinafter. The MAE has been chosen as a performance indicator because the often-used root-mean-square error (RMSE) is sensitive to outliers. Consequently, the MAE is more reliable than the RMSE to assess the average model-performance error as suggested by the authors of reference [9].

Fig. 4 (a) shows the DNI of four consecutive days from the annual simulation, whereby the sky during day one is clear in the morning and overcast in the afternoon. Day two and four represent a day with lightly overcast sky and day three outlines the DNI of a typical day with no cloud cover. Fig. 4 (b) depicts the corresponding absorbed thermal power of the HTF and heat losses of the whole solar field in the case of Solar Salt. Although the design heat losses of the model are higher than SAM's, they are underestimated during the simulation which, in return, results in increased absorbed power of the HTF. This can mainly

be attributed to the two different calculation approaches and the reliance of the empirical heat loss model on merely the absorber surface temperature. As the heat losses of the receiver tube used in this study were determined empirically, it can be assumed that the model presented here is more accurate for this specific receiver type and that SAM is overestimating the heat losses. However, Fig. 4 (c) shows that the lower heat losses of the new model do not significantly affect the SF outlet temperature compared to SAM. In fact, with a MAE of 2.51 °C for Solar Salt (Table 4) the model shows a good agreement with the results from SAM. Likewise, the MAE of the flow rate in the case of Solar Salt is similarly low with 0.13 kg/s. The highest MAE can

Parameter	Unit	Solar Salt	Hitec	Hitec XL
Outlet temperature	°C	2.51	3.64	4.67
Absorbed power	MW_{th}	1.34	2.84	2.91
Heat loss	MW_{th}	2.48	3.37	3.43
Flow rate	kg/s	0.13	0.32	0.31

Table 4. Mean absolute errors (MAE) between the model and SAM for various HTFs
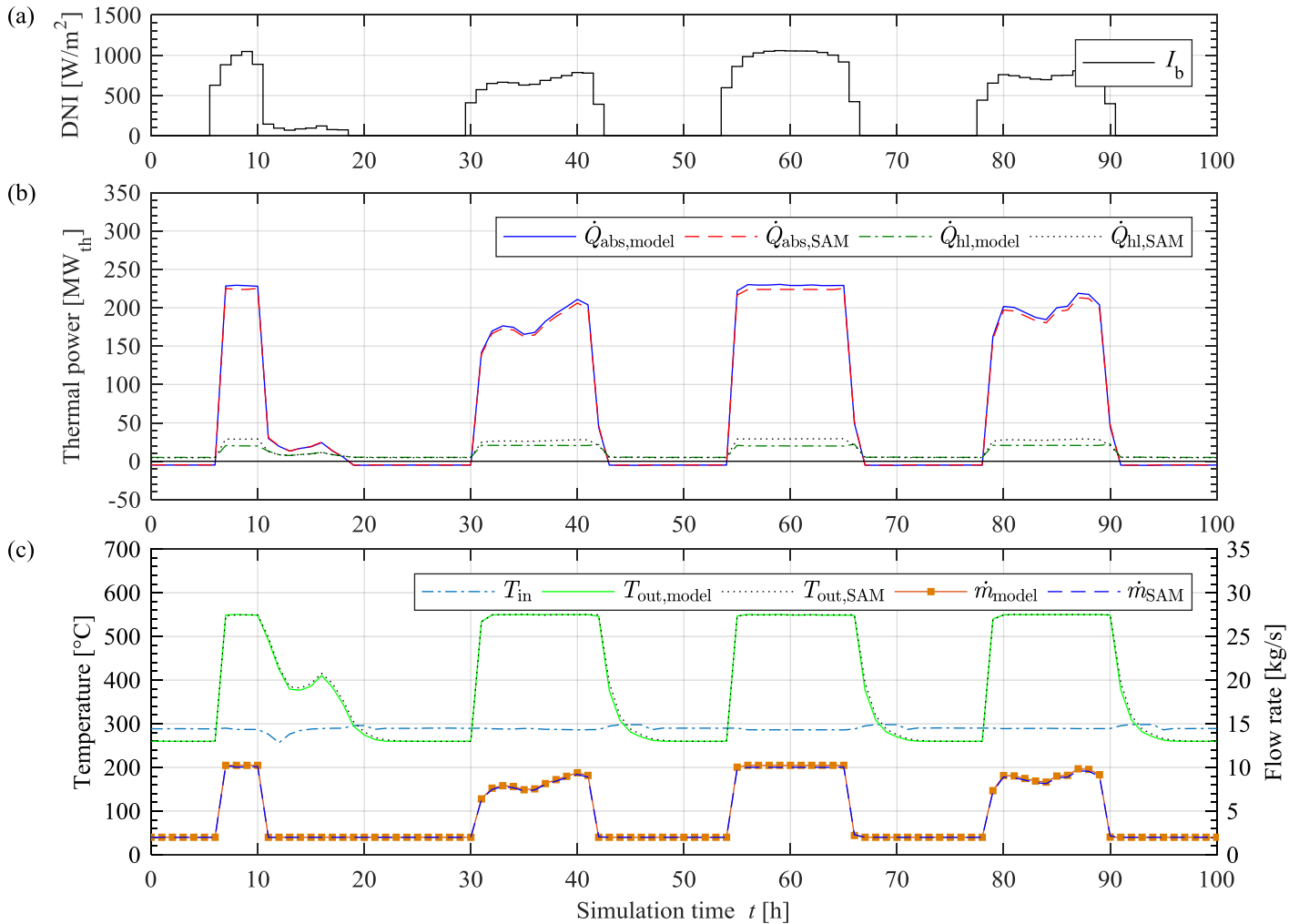

Fig. 4. Comparison of (a) the DNI used in both models, (b) absorbed thermal power and heat losses of the SF, and (c) SF temperatures and flow rates from SAM and the new model for Solar Salt with a time step size of 60 min and 1 CV per SCA
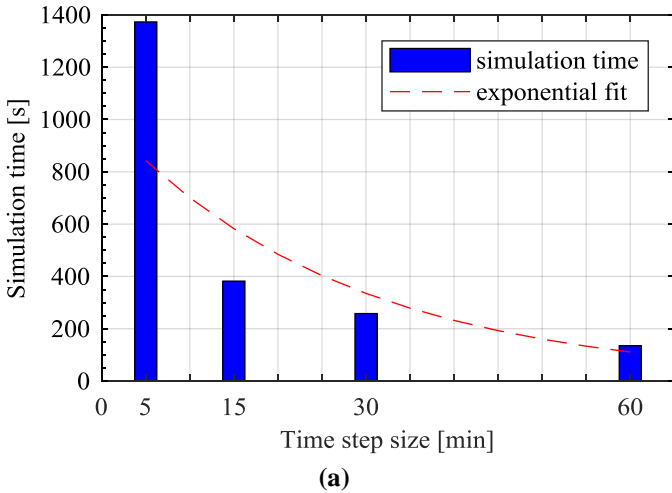
be observed for Hitec XL where the MAE of the outlet temperature is 4.67 °C which can be attributed to the high difference in heat losses between the model and SAM.

4. Model improvements

As the intended use of the model is multi-objective optimization studies with the Dynamic Energy System Optimizer (DYESOPT) developed by KTH [10], several changes were necessary to ensure that the model is well suited for this purpose and to reproduce reliable outputs.

4.1. Parameter study

As high computational effort is a limiting factor for multi-objective optimizations, any reduction in simulation time is beneficial. Thus a parameter study has been carried out to investigate the effect of the time step size and number of control volumes per SCA on the simulation time. The MAE has been chosen as a performance indicator to facilitate a trade-off

between model accuracy and simulation speed. Fig. 5 (a) shows the effect of different time step sizes on the simulation time, which decreases more than exponentially for increasing time step sizes. All evaluations were performed with one control volume per SCA. Fig. 6 (a) shows a significant reduction of the MAE for the outlet temperature and a slight reduction of the MAE for the heat losses and absorbed thermal power when increasing the time step size. Hence, a higher temporal resolution is recommended as it reduces both, the simulation time and the MAE. Still, it has to be noted that these results show a comparison of the results from the new model to the output from SAM for the same corresponding time step sizes and any errors and uncertainties within SAM also reflect in the results in Fig. 6 (a). To eliminate the uncertainties related to the accuracy of the new model, a comparison to real measurement data is necessary and will be done in a future study. However for the purpose of this study, the present results are satisfactory.

A linear increase in simulation time for increasing levels of discretization per SCA can be observed in Fig. 5 (b), whereas
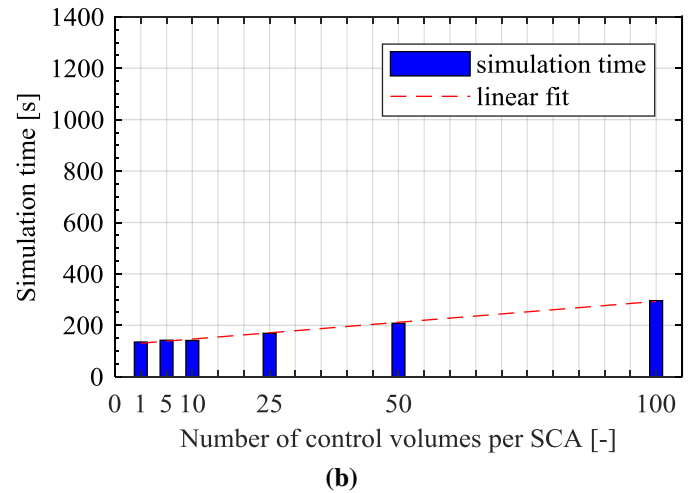

Fig. 5. Simulation time for increasing (a) time step sizes and (b) levels of discretization per SCA
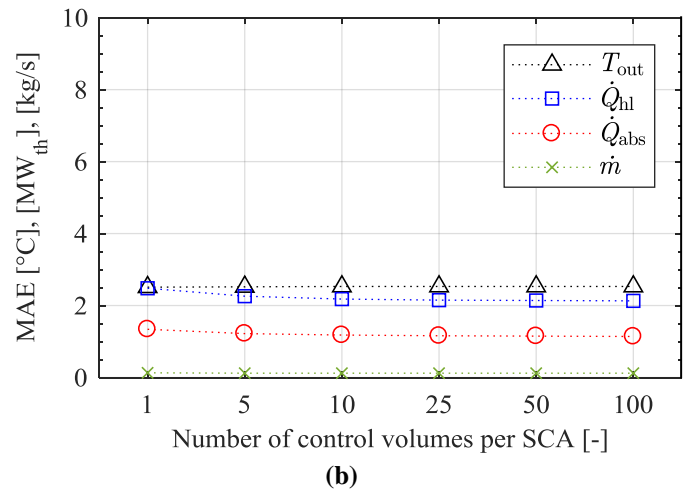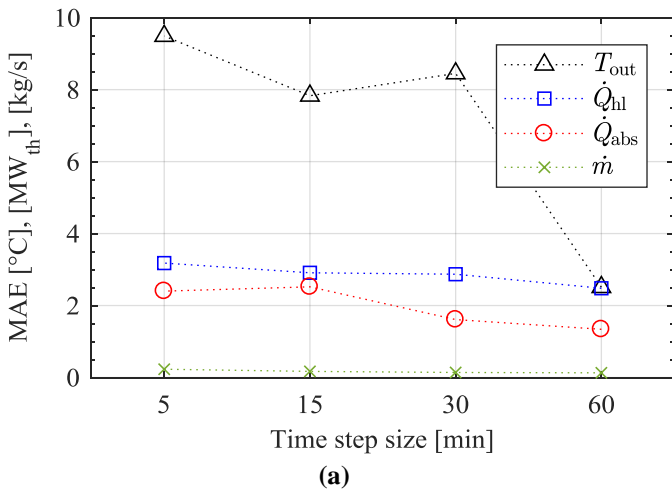

Fig. 6. Mean absolute errors for increasing (a) time step sizes and (b) number of control volumes per SCA

Fig. 6 (b) depicts the resulting reduction of the MAE when increasing the number of control volumes per SCA. Although the MAE for the outlet temperature and flow rate remains constant, the MAE for the heat losses and in turn the absorbed thermal power is reduced. Nonetheless, the gained accuracy through a higher level of discretization does not justify the resulting increased simulation time so that one control volume per SCA is sufficiently accurate for the model.

4.2. Model adaptation

Because SAM was originally developed for the use of thermal oils as HTF, it is not completely suitable for molten salts due to their special characteristics and requirements. Therefore, the following changes and improvements have been implemented in the model.

Firstly, it is not possible to provide an empirical value for the thermal inertia for every examined power plant during a multi-

objective optimization with several thousand different power plant configurations. Therefore, the first improvement was to change the terms for the thermal inertia of the solar field piping to their respective estimated steel masses rather than an empirical value as per the implementation in SAM, eliminating the uncertainty of the empirical thermal inertia values.

Secondly, SAM assumes to recirculate the HTF at night from the SF outlet directly back to the SF inlet which accelerates the cool down of the HTF. This method is not suitable for molten salts due to their high freezing temperature. Thus, a recirculation from the cold storage tank was implemented. The cooler HTF is pumped from the SF outlet to the cold tank and hot fluid from the storage is then pumped into the SF inlet. This allows the usage of the stored energy during night time and reduces the need for electric freeze protection like trace heating [11].

Thirdly, a night time flow rate of 4 kg/s has been introduced to guarantee that the salt is not falling below the freezing
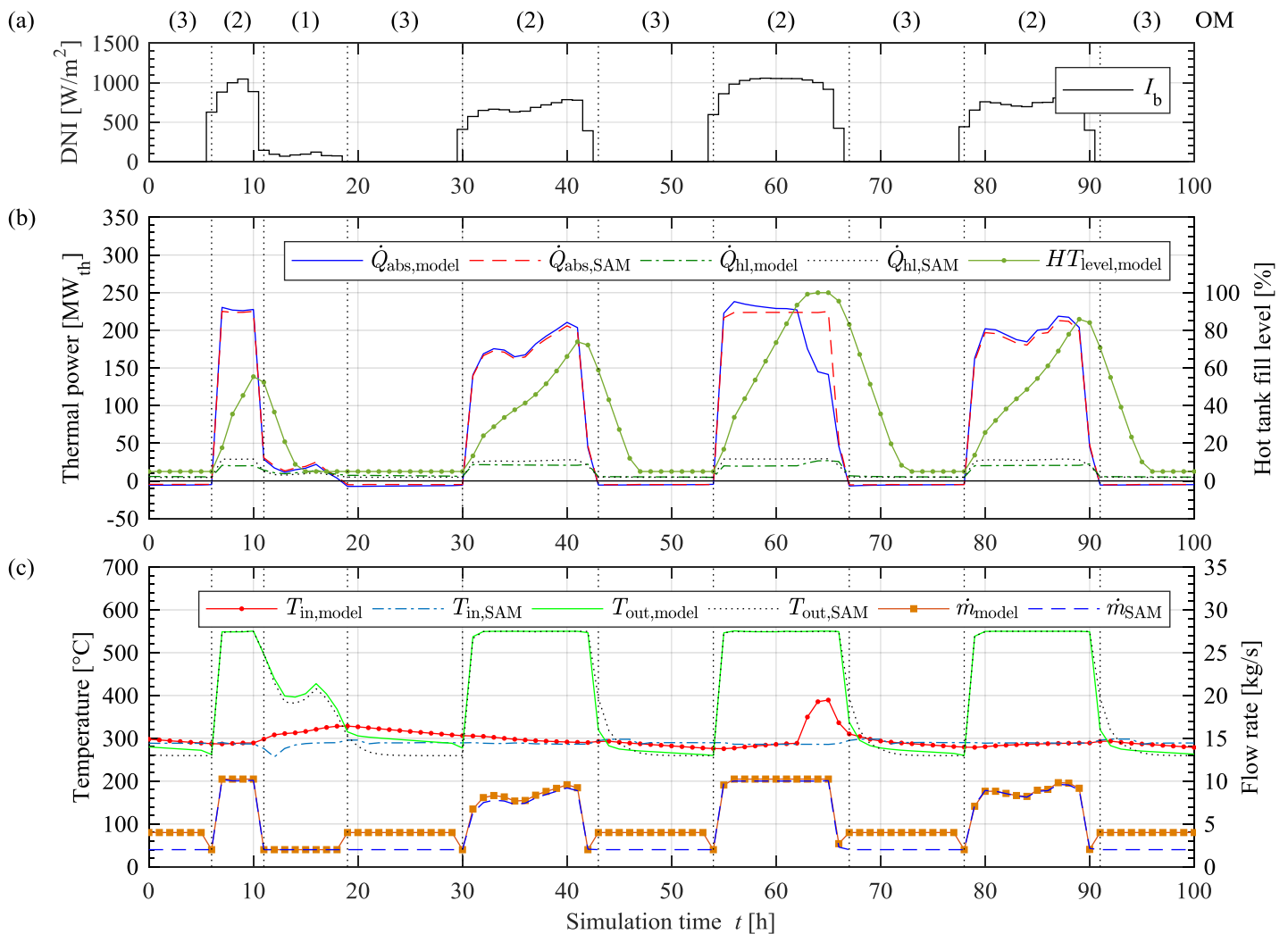

Fig. 7. Comparison of (a) the DNI used in both models, (b) absorbed thermal power, heat losses and hot tank fill level, and (c) SF temperatures and flow rates from SAM and the new model for Solar Salt with the corresponding operating modes

temperature. Although the heat transfer coefficient increases in that case, the same flow rate is used in Archimede Solar Energy's test loop [12] to avoid freezing of the HTF.

The effect of these improvements on the performance of the SF can be seen in Fig. 7. The absorbed thermal power of the HTF in Fig. 7 (b) shows a dip at the end of day three because the hot tank (HT) is fully charged. The underlying control strategy then redirects the fluid to the cold storage tank, which results in an increase of the solar field inlet temperature in Fig. 7 (c). This, in return, increases the heat losses in the solar field and because the fluid is already relatively hot at the loop inlet (approx. 390 °C), the collectors defocus to prevent the HTF from overheating, resulting in a lower absorbed thermal power. It can also be noted that during a day with low solar resource (day one), the solar field changes to operation mode (1) and directs the hot fluid to the cold storage tank because it is not hot enough for the HT. The resulting increase of the cold storage tank temperature keeps the fluid temperature above the minimum allowable value during the night operation mode (3) and eliminates the need for freeze protection in this case. The effect of the increased night flow rate can be seen at the end of the night at hour 29, where the solar field control is switched to operating mode (2), resulting in a drop of the outlet temperature.

5. Conclusion

The model developed in this study shows high agreement with SAM for all three investigated heat transfer fluids. The empirical heat loss model was found to be accurate and eliminates the need of a more complex and time consuming heat loss calculation. The parameter study showed that one control volume per SCA reduces simulation time and at the same time provides sufficiently accurate results. A time step size of 60 minutes reduces both, the simulation time and MAE. However, a validation study with real measurement data is recommended to eliminate remaining uncertainties of the accuracies related to the variation of the time step size and will be carried out in a future study. Various adaptations have been implemented in the model to facilitate molten salts and their operation requirements. The results show that the recirculation from the cold tank keeps the fluid temperature above the freeze protection temperature during some nights and thus reduces the need for electric heat tracing.

Acknowledgements

References

[1] NREL, SAM (System Advisor Model), V2017.9.5 (Revision 2), (2017). https://sam.nrel.gov/.

[2] NREL, System Advisor Model (SAM) Case Study: Gemasolar, (2013) 1–10. https://sam.nrel.gov/sites/sam.nrel.gov/files/content/case_studies/sam_case_csp_physical_trough_andasol-1_2013-1-15.pdf (accessed May 20, 2015).

[3] F. Zaversky, R. Medina, J. García-Barberena, M. Sánchez, D. Astrain, Object-oriented modeling for the transient performance simulation of parabolic trough collectors using molten salt as heat transfer fluid, Sol. Energy. 95 (2013) 192–215. doi:10.1016/j.solener.2013.05.015.

[4] F. Matino, A. Maccari, Molten Salt Receivers Operated on Parabolic Trough Demo Plant and in Laboratory Conditions, Energy Procedia. 69 (2015) 481–486. doi:10.1016/j.egypro.2015.03.056.

[5] M. Gálvez-Carrillo, R. De Keyser, C. Ionescu, Nonlinear predictive control with dead-time compensator: Application to a solar power plant, (2008). doi:10.1016/j.solener.2008.11.005.

[6] M.J. Wagner, P. Gilman, Technical Manual for the SAM Physical Trough Model, Golden, Colorado, 2011. http://www.nrel.gov/docs/fy11osti/51825.pdf.

[7] Archimede Solar Energy, HCEMS-11 Molten Salts - Product Specification, (2017). http://www.archimedesolarenergy.it/en_specifiche-prodotto-hcems-11.htm (accessed July 17, 2017).

[8] Y.-T. Wu, C. Chen, B. Liu, C.-F. Ma, Investigation on forced convective heat transfer of molten salts in circular tubes, Int. Commun. Heat Mass Transf. 39 (2012) 1550–1555. doi:10.1016/j.icheatmasstransfer.2012.09.002.

[9] C.J. Willmott, K. Matsuura, Advantages of the mean absolute error (MAE) over the root mean square error (RMSE) in assessing average model performance, Clim. Res. 30 (2005) 79–82.

[10] J.D. Spelling, Hybrid Solar Gas-Turbine Power Plants: A Thermoeconomic Analysis, KTH Royal Institute of Technology. Stockholm, Sweden, 2013.

[11] C.A. Pan, D. Ferruzza, R. Guédez, F. Dinter, B. Laumert, F. Haglind, Identification of Optimum Molten Salts for Use as Heat Transfer Fluids in Parabolic Trough Plants. A Techno- Economic Comparative Optimization, in: SolarPACES 2017, Santiago, Chile, 2017.

[12] A. Maccari, D. Bissi, G. Casubolo, F. Guerrini, L. Lucatello, G. Luna, A. Rivaben, E. Savoldi, S. Tamano, M. Zuanella, Archimede Solar Energy Molten Salt Parabolic Trough Demo Plant: A Step Ahead towards the New Frontiers of CSP, Energy Procedia. 69 (2015) 1643–1651. doi:10.1016/j.egypro.2015.03.122.